Nanoscale

Exciton-dipole coupling in two-dimensional rubrene assembly sensors

Journal:	*Nanoscale*
Manuscript ID	NR-ART-12-2018-010373.R1
Article Type:	Paper
Date Submitted by the Author:	25-Feb-2019
Complete List of Authors:	Guan, Yingshi; University at Buffalo - The State University of New York, Hu, Feng; University at Buffalo - The State University of New York Li, Changning; University at Buffalo - The State University of New York Ren, Shenqiang; University at Buffalo - The State University of New York,

Journal Name

ARTICLE

Exciton-dipole coupling in two-dimensional rubrene assembly sensors

Received 00th January 20xx,
Accepted 00th January 20xx

DOI: 10.1039/x0xx00000x

www.rsc.org/

Ying-Shi Guan[a,b], Feng Hu[a,b], Changning Li[a,b], Shenqiang Ren[a,b*]

The selective detection of molecules with less energy consumption depends critically on the novel sensing concepts and emergence of new sensor materials. Excitons and dipole moments are two strongly correlated states that have shown the coupled electronic interactions at the nanoscale, highly sensitive to the changes in their surroundings. Here, we present the exciton-dipole coupling in two-dimensional (2D) assembly of molecular rubrene excitonic crystals to selectively detect molecules. The presence of molecules with a dipole moment transforms excitons into charge transfer, resulting in a pronounced conductivity change of freestanding rubrene nanosheets. The exciton-dipole coupling exhibits a highly efficient molecular selectivity, as it offers an unambiguous electronic fingerprint for the detection of molecules - in contrast to common sensing schemes relying on the quantification of intensity changes and optical peak shifts.

1 Introduction

Molecular sensing of chemical substances has been extensively investigated, which reveals that the well-designed host structures are essential for high sensitivities and selectivities[1-4]. Among the various types of sensors, resistive sensors - also known as Taguchi sensors - are the most attractive one due to the low cost, short response time, simple operation and wide application[5]. In this context, a porous semiconductor layer (e.g. tin dioxide [SnO_2][6], tungsten trioxide [WO_3][7], titanium dioxide [TiO_2][8], and zinc oxide [ZnO][9,10]) becomes responsive at an elevated temperature up to a few hundred degrees. To meet the sensing requirements under ambient condition with energy-saving, highly selective and sensitive features, it is highly desirable to develop a novel sensor device based on more promising material and mechanism[2,11-13]. One class of these materials is the two-dimensional (2D) assembly of molecular excitonic crystalline nanosheets (ECNs), due to their unique features including the large surface and orderly anisotropy enabling the high sensitivity and superior selectivity. However, ECNs exhibit tightly-bound excitons due to their strong Coulomb interaction, direct band gap and extended conjugated pi-electronic structure. Here, we show that charge transfer can be induced by an efficient exciton-dipole coupling interaction between the ECN and a guest molecule with a specific dipole moment which are non-covalently attached onto the sheets, enabling a read-out electrical signal. The output signal highly depends on the intensity of charge transfer from the ECNs to guest molecules. The electrical response of ECNs towards the specific molecule shows a great potential in fabrication of flexible sensors for the selective detection of target molecules.

Conjugated organics have been widely explored for the sensor materials due to their high tunability in conductivity through the redox interaction with target molecules[5,14-19]. Such interaction between sensor materials and target molecules mainly take place on the surface, and hence, the unique nanostructured morphologies (tubes, wires, nanosheets, etc) through chemical method show large surface-to-volume ratio and high specific surface area, which is critical for the sensor performance[2,3,20-22]. In this work, we report a water-air interfacial assembly method to control the crystallization and molecular packing to fabricate pseudo-2D rubrene crystalline nanosheet, an exemplary ECN material[23]. The freestanding molecular rubrene ECNs can serve as molecular sensor to employ the exciton-dipole coupling for the selective detection of molecules with a specific dipole moment.

2 Experimental section

2.1 Materials and instruments.

Rubrene and P3BT were purchased from Sigma-Aldrich and used as received. The SEM images were taken from FEI Quanta450FEG. UV-Vis spectrum was recorded on an Agilent Model HP8453 UV-vis spectrophotometer. Keithley 2400 SourceMeter was used in order to obtain current versus voltage curves. A Bruker Apex II Duo single-crystal X-ray diffractometer was used to obtain the XRD pattern at a step of 0.3° per minute from 3°to 30°. Light dependent current measurement and current-voltage (I-V) characteristics of the devices are measured in atmosphere condition with a CHI 422 Series Electrochemical Workstation with or without an applied an

[a] Department of Mechanical and Aerospace Engineering, University at buffalo, The State University of New York, Buffalo, NY, 14260, USA
[b] Research and Education in eNergy, Environment and Water (RENEW) Institute, University at buffalo, The State University of New York, Buffalo, NY, 14260, USA
E-mail: shenren@buffalo.edu

Electronic Supplementary Information (ESI) available: See DOI: 10.1039/x0xx00000x

illumination from OSL2 fiber illuminator calibrated by Newport Power Meter with Model 1918-R.

2.2 Rubrene nanosheets fabrication.

10 mg rubrene were dissolved in 1 mL Toluene. Drop 100 uL solution onto the surface of DI water, then the organic solution spreads spontaneously and rapidly onto the water surface due to the Marangoni effect. After several minutes, the uniform nanosheet can be formed over large area. The obtained nanosheet can be transferred onto any substrates such as silicon, glass, PDMS and so on.

2.3 Device fabrication.

Fabrication of Horizontal devices on ITO substrates: Patterned ITO substrate with different channel width (50um, 75um, 100um, 150um and 200um) were sonicated continuously in sofa water, distilled water, acetone and Isopropyl Alcohol for 10 min and then blown dry by N2. The substrates were then irradiated by oxygen plasma for 10 min. The fabricated rubrene nanosheets on water surface were transferred onto the substrates. The devices were naturally air-dried overnight. Then the devices were dried at 100°C for 60 min in glovebox.

3 Results and discussion

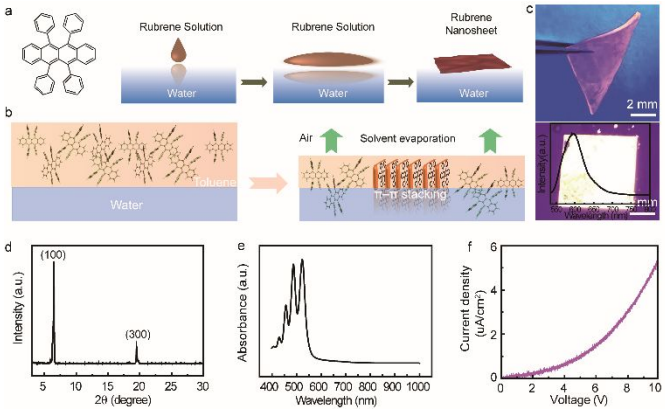

Figure 1 (a-b) The chemical structure of rubrene molecule and the schematic illustration of self-assembly approach to grow the freestanding rubrene nanosheet at the water-air interface. (c) The photograph of the freestanding rubrene nanosheets on PDMS substrate and glass substrates illuminated by UV lamp and the photoluminescence spectrum of rubrene nanosheet, the scale bar is 2 mm. (d) The XRD patterns of rubrene nanosheets. (e) The UV-Vis absorption spectrum of rubrene nanosheets. (f) The I-V curve of rubrene nanosheets.

When the rubrene solution is dropped onto the water surface, it spreads spontaneously and rapidly onto the water surface due to the Marangoni effect (Figure 1a). The high-quality and uniform nanosheet can be formed over large area after the evaporation of solvent, where the aggregation and nucleation of rubrene molecules are driven by the π–π stacking, and hydrophobic interactions (Figure 1b). The freestanding pseudo-2D rubrene nanosheet grow in the lateral direction with the dimension of ~10 cm^2. Figure S1 shows the typical freestanding rubrene nanosheet floating on the DI water. The obtained high-quality and uniform ECNs can be transferred onto any artificial surface and structure, such as silicon, glass, aluminum foil, polydimethylsiloxane, and so on (Fig. 1c and Fig. S1). The optical image of rubrene nanosheet (Fig.S2) shows a large-area and continuous morphology with a smooth surface and sharp edge. The scanning electron microscopy (SEM) image further confirm the flat and uniform morphology of 2D rubrene nanosheet with partially folded sheets (Fig. S3). Figure 1d shows the X-ray diffraction (XRD) pattern of the as-grown rubrene nanosheets, exhibiting highly crystalline nature. The strong diffraction peaks at 6.5° and 19.5° correspond to (100) and (300) plane, respectively, which are consistent with the single crystal rubrene diffraction[24-26]. The absorption spectrum (Fig. 1e) of rubrene nanosheets exhibits the characteristic ??? electronic absorbance peak at 522 nm (2.37 eV) along with the progressive vibronic bands associated with C-C stretching[27]. When irradiated by UV lamp, the freestanding rubrene ECNs show a strong fluorescence. The freestanding rubrene ECN nanosheets provide advantageous access to understand the electronic properties resulted from its long-range-ordered packing. The conductivity of rubrene nanosheets can reach up to 2.36 X 10^{-6} S/cm (Figure 1f), which can be exploited for further sensing studies.

The exciton-dipole coupling on electronic properties of rubrene-ECNs is largely influenced by the molecular dipole moment and its non-covalent surface coverage. To exploit the exciton-dipole interactions between rubrene ECNs and non-covalently attached molecules, we apply the freestanding rubrene ECNs as the miniaturized resistive sensors for the real-time detection of NH3 (the dipole moment of 1.42 D), ethanol (1.69 D) and acetone (2.91 D). As shown in Figure 2a, the current density of freestanding rubrene ECNs is increased dramatically as exposing to NH_3, ethanol, and acetone vapor environment. The time-dependent measurements show that the rubrene ECNs exhibit fast response and recovery on the cyclic exposure to 100 ppm of NH_3, ethanol, and acetone vapor (Figure 2b). While the rubrene ECNS are exposed to target molecules with weak dipole moment, such as hexane (0.08 D), benzene (0 D), toluene (0.36 D), and p-dichlorobenzene (0 D), the current densities show negligible changes, verifying that the strong dipole moment accounts for the electrical response (Figure S8). The proposed sensing mechanism for the rubrene ECNs serving as molecular sensor is therefore depicted in Figure 2c, in which each NH3, ethanol, and acetone molecule has one lone pair of electrons to facilitate the dipole moment, leading to the strong exciton-dipole interactions. The exciton-dipole interactions between the rubrene ECNs and attached molecules facilitate the charge transfer behavior, leading to the change in the conductivity of rubrene ECNs.

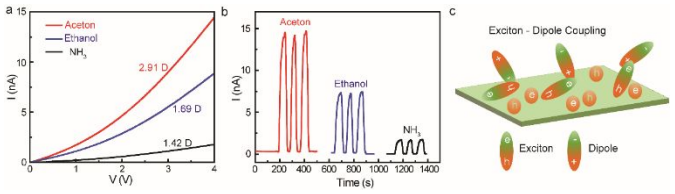

Figure 2 (a) The I-V curves of the rubrene nanosheets when exposed to acetone, ethanol, and ammonia vapor with a dipole moment of 2.91 D, 1.69 D, and 1.42 D, respectively. (b) The time dependent current measurements of the rubrene nanosheets when

exposed to acetone, ethanol, and ammonia vapor. (c) The proposed sensing mechanism of rubrene nanosheets.

To further verify our hypothesis, we carried out the Raman test for the rubrene nanosheets, where Raman frequencies and intensities are experimental observables emerging directly from the π-conjugated backbone. Figure S9 shows the Raman spectra of rubrene nanosheets before and after ethanol exposure, as excited with 785 nm-laser. The main typical resonance bands of rubrene are observed at the reported frequencies (1003, 1034, 1166, 1301, 1597, 1621, cm^{-1}). These Raman active modes showed the signature of crystalline rubrene reported in literatures. A visible increase can be observed in the intensity after ethanol gas adsorption, revealing that the coupling between rubrene exciton and gas molecule dipoles. Furthermore, the absorption spectra of rubrene nanosheet show the subtle difference before and after gas adsorption (Figure S10), while the intensity of emission spectra of rubrene exhibited the decrease after gas adsorption. The fluorescence of the rubrene was quenched dramatically after gas adsorption through charge (electron) transfer[29,30]. These results reveal that the ethanol gas molecules (dipoles) interact with rubrene molecules, leading to the change in the carrier density of rubrene ECNs.

The molecules are non-covalently attached to the surface of rubrene ECNs, implying that their electronic wave function remains unchanged to a large extent after molecular adsorption. Therefore, we employ the charge-transfer complex ECNs, consisting of electron donor and acceptor, to examine the exciton-dipole interaction when the molecules induce a static dipole field. Here we select tetracyanoquinodimethane (TCNQ) and C_{60} as electron acceptor molecules to form the charge transfer complex with rubrene for further studies. As shown in Figure 3a, the time-dependent current measurement shows that the freestanding rubrene-TCNQ nanosheet exhibits a faster response and recovery on the cyclic exposure to 100 ppm of ethanol than that of rubrene-C_{60}. As a comparison, the sensing performance of a commercial ethanol oxide sensor is investigated under the same condition. Although the commercial sensor has a lower response time, its time-dependent current change of the commercial sensor shows a long recovery time of 33.1 s when exposed to 100 ppm ethanol vapor, significantly higher than the ones of rubrene-TCNQ (3.9 s) and rubrene-C_{60} (12.3 s) ECNs. Meanwhile, the sensor fabricated by rubrene-TCNQ ECNs also has a shorter response time 3.8 s smaller than that of rubrene-C_{60}. The difference in response and recovery time between these two kinds of devices is caused by the different energy band structures of the TCNQ and C_{60}. As shown in Figure 3b, TCNQ has a lower unoccupied molecular orbital (LUMO) energy level than that of C_{60}, which facilitates the formation of charge-transfer complex with rubrene molecules. When exposed to the target molecules with a large dipole moment, the excitons can be converted into a large density of free charge carriers, leading to an enhanced conductivity and a short response time, which plays a dominant role in the sensor performance. The sensitivity of rubrene ECN sensor can be defined as I_g/I_a, where the I_g and I_a are the current of the sensor in gas and air plotted in Figure 3c. the devices based on rubrene-TCNQ and rubrene-C_{60} nanosheets show the sensitivity value of 75 and 56, respectively, higher than that of the devices by pure rubrene nanosheets with a value of 45. However, the commercial sensor has the lowest sensitivity with a value of 6. Moreover, the commercial ethanol sensor shows poor selectivity towards other common molecules, including hexane, acetone, benzene, toluene, dichlorobenzene, and NH_3 (Figure S4-7). In addition, the current density-voltage (I-V) curves of the rubrene-TCNQ ECNs are measured under different concentrations of ethanol vapor (Figure 3d). The current of freestanding rubrene-TCNQ ECNs is increased dramatically from 1.7 nA to 101 nA at the applied potential 4.5 V, when exposed to increased concentration of the ethanol vapor from 10 ppm to 1000 ppm. The time-dependent measurements indicate that the rubrene-TCNQ ECNs exhibit quick and repeatable response and recovery on the cyclic exposure to ethanol vapor with different concentrations (Figure 3e). It should be noted that the sensor response follows a good linear trend over a wide range of ethanol level, as shown in Figure 3f. The linear dependent equation is illustrated in supporting information. We attribute this result to the unique exciton-dipole interaction, which allow the sensor response and recovery to reach the equilibrium with a completely reversible behavior. In the meantime, as the ethanol vapor concentration increases, the density of free charge carriers generated from the exciton-dipole interaction is increased, leading to the linear dependence of ethanol vapor concentration.

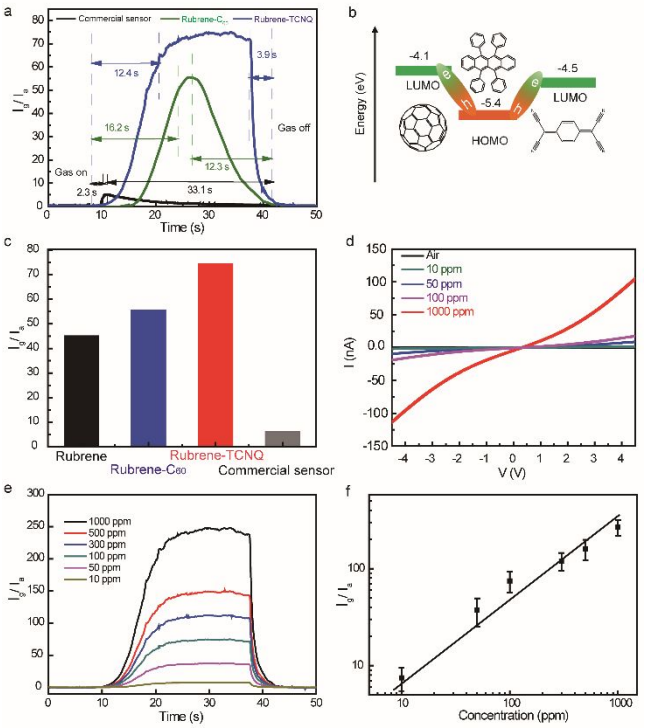

Figure 3 (a) The determination of response and recovery time of the sensing devices based on rubrene-TCNQ and rubrene-C60 nanosheets and the commercial sensor when exposed to 100 ppm of ethanol vapor. (b) Schematic energy level diagram of C60, Rubrene, and TCNQ, demonstrating electrons from the HOMO of the donor molecules transfer into the LUMO of the acceptor molecules. (c) The detectivity (I_g/I_a) values of the sensors fabricated by pure rubrene, rubrene-TCNQ, and rubrene-C60 nanosheets and

the commercial sensor. (d) The I-V curves of the rubrene-TCNQ nanosheets when exposed to different concentration of ethanol vapor. (e) The time dependent current measurements of the rubrene-TCNQ nanosheets when exposed to different concentrations of ethanol vapor. (f) The detectivity value of the Rubrene-TCNQ sensor dependent on the concentration of ethanol vapor.

A flexible and stretchable sensor platform would be interesting to explore the applications of exciton-dipole interaction mediated sensors in extreme environments. Therefore, we transfer freestanding rubrene-TCNQ ECNs onto the polydimethylsiloxane substrate to fabricate the flexible and stretchable sensor device, as depicted in Figure 4a. The current of flexible sensor devices is increased dramatically from 0.8 to 7.2 nA at the applied potential of 5 V when exposed to an increased concentration of ethanol vapor from 10 to1000 ppm (Figure 4b), verifying its superior sensitivity. Meanwhile, due to the good flexibility and stability, its electronic read-out currents from the I-V measurements of the sensor exposed to 100 ppm of ethanol vapor show a negligible difference from the relax status to bending one (Figure 4c). After a cyclic bending of the sensor with more than 200 bending-relax cycles (Figure 4d), the sensor can nearly maintain a constant output current. This result demonstrates that the good reversibility and reproducibility of the flexible sensor. The kirigami-inspired structure is further introduced to improve the stretchability of flexible sensor as the scaffold[23,28]. The freestanding nanosheets are transferred onto the tracing paper and then cut into a selective kirigami structure by laser. As shown in Figure 4e, the kirigami-inspired flexible sensor can be stretched up to 100% with a negligible change in conductance. The current-voltage (I-V) curves of the kirigami ECN nanosheets at different strains (Figure 4e) show no decrease in conductivity during the entire stretching process. More importantly, the detectivity of the kirigami-inspired flexible sensor only has a slight change of the I_g/I_a value smaller than 3.0% when being stretched up to 100% strain from the original status. These results reveal that the kirigami-inspired stretchable sensor provide potential in the application of flexible and stretchable sensing devices.

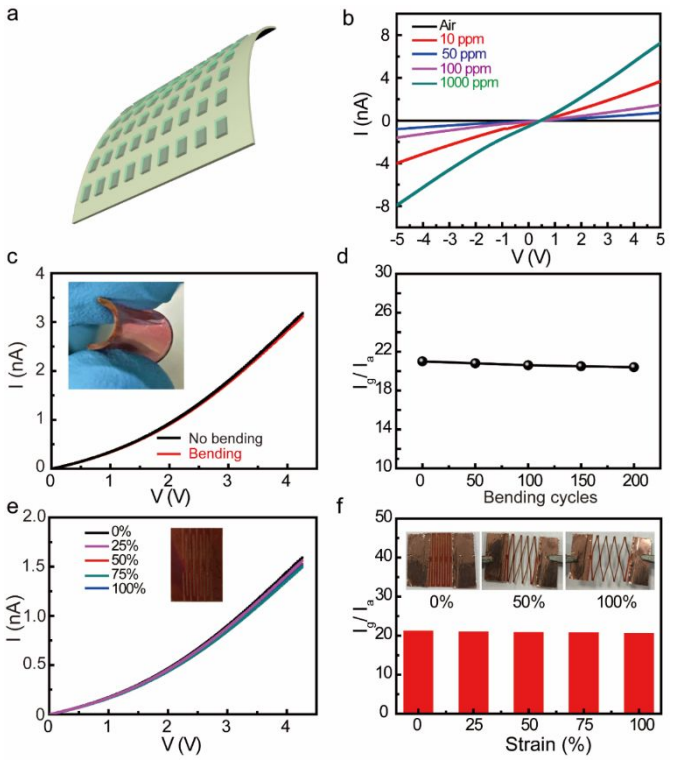

Figure 4 (a) The schematic diagram of the flexible rubrene sensor. (b) The I-V curves of the flexible rubrene sensor on PDMS substrates when exposed to different concentrations of ethanol vapor. (c) The I-V curves of the flexible rubrene sensor on PDMS substrates with bending and without bending when exposed to 100 ppm ethanol vapor. (d) Bending cycles test of the flexible rubrene sensor on PDMS showing that the detectivity has a negligible degradation. (e) The I-V curves of the kirigami-inspired rubrene sensor at different strain when exposed to 100 ppm ethanol vapor. (f) The detectivity of the kirigami-inspired rubrene sensor at different strain when exposed to 100 ppm of ethanol vapor.

4 Conclusions

In conclusion, a scalable water-air interfacial assembly method is developed to grow freestanding molecular rubrene ECNs. The freestanding molecular rubrene ECNs can serve as molecular sensor to employ the exciton-dipole coupling for the selective detection of molecules with a specific dipole moment. The time-dependent measurements show that the rubrene charge-transfer ECNs exhibit a short response and recovery time as well as superior sensitivity, which can be attributed to the unique exciton-dipole coupling mechanism. This new sensing mechanism allow the sensor response and recovery to reach the equilibrium with a completely reversible behavior and linear dependence. More importantly, the kirigami-inspired rubrene sensors enable the stretchability of 100% with negligible change in detectivity, which can provide a platform to develop flexible and stretchable sensing devices. The exciton-dipole coupling interactions obtained through freestanding ECNs and non-covalently attached molecules can serve as a new sensing mechanism for the selective detection of molecules with the dipole moment.

Conflicts of interest

There are no conflicts of interest to declare.

Acknowledgements

Work (S.R.) was supported by Army Research Office (W911NF-18-2-0202).

References

1 Janata, J.; Bezegh, A. Chemical Sensors. Anal. Chem. 1988, 60, 62−74.
2 Zhang, J.; Liu, X.; Neri, G.; Pinna, N. Nanostructured Materials for Room-Temperature Gas Sensors. Adv. Mater. 2016, 28, 795−831.
3 Schedin, F.; Geim, A. K.; Morozov, S. V.; Hill, E. W.; Blake, P.; Katsnelson, M. I.; Novoselov, K. S. Detection of Individual Gas Molecules Adsorbed on Graphene. Nat. Mater. 2007, 6, 652−655.
4 Jariwala, D.; Sangwan, V. K.; Lauhon, L. J.; Marks, T. J.; Hersam, M. C. Carbon Nanomaterials for Electronics, Optoelectronics, Photovoltaics, and Sensing. Chem. Soc. Rev. 2013, 42, 2824−2860.
5 Smulko, J. M.; Trawka, M.; Granqvist, C. G.; Lonescu, R.; Annanouch, F.; Llobet, E.; Kish, L. B. New Approaches for Improving Selectivity and Sensitivity of Resistive Gas Sensors: A Review. Sens. Rev. 2015, 35, 340−347.
6 Paulowicz, I.; Hrkac, V.; Kaps, S.; Cretu, V.; Lupan, O.; Braniste, T.; Duppel, V.; Tiginyanu, I.; Kienle, L.; Adelung, R.; Mishra, Y. K. Three-Dimensional SnO2 Nanowire Networks for Multifunctional Applications: From High-Temperature Stretchable Ceramics to Ultraresponsive Sensors. Adv. Electron. Mater. 2015, 1, 1500081.
7 Meng, Z.; Fujii, A.; Hashishin, T.; Wada, N.; Sanada, T.; Tamaki, J.; Kojima, K.; Haneoka, H.; Suzuki, T. Morphological and Crystal Structural Control of Tungsten Trioxide for Highly Sensitive NO2 Gas Sensors. J. Mater. Chem. C 2015, 3, 1134−1141.
8 Bai, J.; Zhou, B. Titanium Dioxide Nanomaterials for Sensor Applications. Chem. Rev. 2014, 114, 10131−10176.
9 Polarz, S.; Roy, A.; Lehmann, M.; Driess, M.; Kruis, F. E.; Hoffmann, A.; Zimmer, P. Structure–Property–Function Relationships in Nanoscale Oxide Sensors: A Case Study Based on Zinc Oxide. Adv. Funct. Mater. 2007, 17, 1385−1391.
10 Kumar, R.; Ai-Dossary, O.; Kumar, G.; Umar, A. Zinc Oxide Nanostructures for NO2 Gas–Sensor Applications: A Review. Nano-Micro Lett. 2015, 7, 97−120.
11 Rana, M. M.; Ibrahim, D. S.; Asyraf, M. R. M.; Jarin, S.; Tomal, A. A review on Recent Advances of CNTs as Gas Sensors. Sens. Rev. 2017, 37, 127−136.
12 Falco, A.; Rivadeneyra, A.; Loghin, F. C.; Salmeron, J. F.; Lugli; P.; Abdelhalimb, A. Towards Low-Power Electronics: Self-Recovering and Flexible Gas Sensors. J. Mater. Chem. A 2018, 6, 7107−7113.
13 Zhang, Z.; Li, H.; Miller, R.; Malissa, H.; Jamali, S.; Boehme, C.; Grossman, J. C.; Ren, S. Freestanding Organic Charge-Transfer Conformal Electronics. Nano Lett. 2018, 18, 4346−4354.
14 Ji, Q.; Honma, I; Paek, S. M.; Akada, M.; Hill, J. P.; Vinu, A.; Ariga, K. Layer-by-Layer Films of Graphene and Ionic Liquids for Highly Selective Gas Sensing. Angew. Chem. Int. Ed. 2010, 49, 9737−9739.
15 Hangarter, C. M.; Chartuprayoon, N.; Hernández, S. C.; Choa, Y.; Myung, N. V. Hybridized Conducting Polymer Chemiresistive Nano-Sensors. Nano Today 2013, 8, 39−55.
16 Wang, T.; Huang, D.; Yang, Z.; Xu, S.; He, G.; Li, X.; Hu, N.; Yin, G.; He, D.; Zhang, L. A Review on Graphene-Based Gas/Vapor Sensors with Unique Properties and Potential Applications. Nano-Micro Lett. 2015, 8, 95−119.
17 Liao, F.; Toney, M. F.; Subramanian, V. Thickness Changes in Polythiophene Gas Sensors Exposed to Vapor. Sens. Actuators, B 2010, 148, 74−80.
18 Huyen, D. N.; Tung, N. T.; Vinh, T. D.; Thien, N. D. Synergistic Effects in the Gas Sensitivity of Polypyrrole/Single Wall Carbon Nanotube Composites. Sensors 2012, 12, 7965−7974.
19 Janata, J.; Josowicz, M. Conducting Polymers in Electronic Chemical Sensors. Nat. Mater. 2003, 2, 19−24.
20 Timmer, B.; Olthuis, W.; Berg, A. V. D. Ammonia Sensors and their Applications—A review. Sens. Actuators, B 2005, 107, 666−677.
21 Huang, X.; Hu, N.; Gao, R.; Yu, Y.; Wang, Y.; Yang, Z.; Kong, E. S.; Wei, H.; Zhang, Y. Reduced Graphene Oxide–Polyaniline Hybrid: Preparation, Characterization and its Applications for Ammonia Gas Sensing. J. Mater. Chem. 2012, 22, 22488−22495.
22 Modi, A.; Koratkar, N.; Lass, E.; Wei, B.; Ajayan, P. M. Miniaturized Gas Ionization Sensors Using Carbon Nanotubes. Nature 2003, 424, 171−174.
23 Guan, Y. S.; Zhang, Z.; Tang, Y.; Yin, J.; Ren, S. Kirigami-Inspired Nanoconfined Polymer Conducting Nanosheets with 2000% Stretchability. Adv. Mater. 2018, 30, 1706390.
24 Zeng, X.; Zhang, D.; Duan, L.; Wang, L.; Dong, G.; Qiu, Y. Morphology and Fluorescence Spectra of Rubrene Single Crystals Grown by Physical Vapor Transport. Appl. Surf. Sci. 2007, 253, 6047−6051.
25 Kanashima, T.; Katsura, Y.; Okuyama, M. Organic Ferroelectric Gate Field-Effect Transistor Memory Using High-Mobility Rubrene Thin Film. Jpn. J. Appl. Phys. 2014, 53, 04ED11.
26 Xie, W.; McGarry, K. A.; Liu, F.; Wu, Y.; Ruden, P. P.; Douglas, C. J.; Frisbie, C. D. High-Mobility Transistors Based on Single Crystals of Isotopically Substituted Rubrene-d28. J. Phys. Chem. C 2013, 117, 11522−11529.
27 O'Malley, S. M.; Amin, M.; Borchert, J.; Jimenez, R.; Steiner, M.; Fitz-Gerald, J. M.; Bubb, D. M. Formation of Rubrene Nanocrystals by Laser Ablation in Liquids Utilizing MAPLE Deposited Thin Films. Chem. Phys. Lett. 2014, 595−596, 171−174.
28 Guan, Y. S.; Li, H.; Ren, F.; Ren, S. Kirigami-Inspired Conducting Polymer Thermoelectrics from Electrostatic Recognition Driven Assembly. ACS nano 2018, 12, 7967−7973.
29 Chen, Y.; Yang, T.; Pan, H; Yuan, Y.; Chen, L.; Liu, M.; Zhang, K.; Zhang, S.; Wu, P.; Xu, J. Photoemission Mechanism of Water-Soluble Silver Nanoclusters: Ligand-to-Metal − Metal Charge Transfer vs Strong Coupling between Surface Plasmon and Emitters. J. Am. Chem. Soc. 2014, 136, 1686−1689.
30 Guan, Y.-S.; Niu, L.-Y.; Chen, Y.-Z.; Wu, L.-Z.; Tung, C.-H.; Yang, Q.-Z. A Near-Infrared Fluorescent Sensor for Selective Detection of Cysteine and its Application in Live Cell Imaging. RSC Adv., 2014, 4, 8360-8364.